

Structural and Functional Characterization of the NHR1 Domain of the *Drosophila* Neuralized E3 Ligase in the Notch Signaling Pathway

Fahu He¹, Kohei Saito¹, Naohiro Kobayashi¹, Takushi Harada¹, Satoru Watanabe¹, Takanori Kigawa^{1,2}, Peter Güntert^{1,3,4}, Osamu Ohara^{5,6}, Akiko Tanaka¹, Satoru Unzai⁷, Yutaka Muto^{1*} and Shigeyuki Yokoyama^{1,8*}

¹RIKEN Systems and Structural Biology Center, 1-7-22 Suehiro-cho, Tsurumi-ku, Yokohama 230-0045, Japan

²Department of Computational Intelligence and Systems Science, Interdisciplinary Graduate School of Science and Engineering, Tokyo Institute of Technology, 4259 Nagatsuta-cho, Midori-ku, Yokohama 226-8502, Japan

³Tatsuo Miyazawa Memorial Program, RIKEN Genomic Sciences Center, Yokohama 230-0045, Japan

⁴Institute of Biophysical Chemistry and Frankfurt Institute of Advanced Studies, Goethe University Frankfurt, Max-von-Laue-Strasse 9, 60438 Frankfurt am Main, Germany

⁵Department of Human Genome Research, Kazusa DNA Research Institute, 2-6-7 Kazusa-kamatari, Kisarazu, Chiba 292-0818 Japan

The Notch signaling pathway is critical for many developmental processes and requires complex trafficking of both Notch receptor and its ligands, Delta and Serrate. In *Drosophila melanogaster*, the endocytosis of Delta in the signal-sending cell is essential for Notch receptor activation. The Neuralized protein from *D. melanogaster* (Neur) is a ubiquitin E3 ligase, which binds to Delta through its first neuralized homology repeat 1 (NHR1) domain and mediates the ubiquitination of Delta for endocytosis. Tom, a Bearded protein family member, inhibits the Neur-mediated endocytosis through interactions with the NHR1 domain. We have identified the domain boundaries of the novel NHR1 domain, using a screening system based on our cell-free protein synthesis method, and demonstrated that the identified Neur NHR1 domain had binding activity to the 20-residue peptide corresponding to motif 2 of Tom by isothermal titration calorimetry experiments. We also determined the solution structure of the Neur NHR1 domain by heteronuclear NMR methods, using a ¹⁵N/¹³C-labeled sample. The Neur NHR1 domain adopts a characteristic β -sandwich fold, consisting of a concave five-stranded antiparallel β -sheet and a convex seven-stranded antiparallel β -sheet. The long loop (L6) between the β 6 and β 7 strands covers the hydrophobic patch on the concave β -sheet surface, and the Neur NHR1 domain forms a compact globular fold. Intriguingly, in spite of the slight, but distinct, differences in the topology of the secondary structure elements, the structure of the Neur NHR1 domain is quite similar to those of the B30.2/SPRY domains, which are known to mediate specific protein–protein interactions. Further NMR titration experiments of the Neur NHR1 domain with the 20-residue Tom peptide revealed that the resonances originating from the bottom area of the β -sandwich (the L3, L5, and L11 loops, as well as the tip of the L6 loop) were affected. In addition, a structural comparison of the Neur NHR1 domain with the first NHR domain of the human KIAA1787 protein, which is from another NHR subfamily and does not bind to the 20-residue Tom peptide, suggested the critical amino acid residues for the interactions between the Neur NHR1 domain and the Tom peptide. The present structural study will shed light on the role of the Neur NHR1 domain in the Notch signaling pathway.

© 2009 Elsevier Ltd. All rights reserved.

*Corresponding authors. S. Yokoyama is to be contacted at the Department of Biophysics and Biochemistry, Graduate School of Science, The University of Tokyo, 7-3-1 Hongo, Bunkyo-ku, Tokyo 113-0033, Japan. E-mail addresses: ymuto@gsc.riken.jp; yokoyama@biochem.s.u-tokyo.ac.jp.

Abbreviations used: D-mib, *Drosophila* Mind bomb protein; GFP, green fluorescent protein; HSQC, heteronuclear single-quantum coherence; ITC, isothermal titration calorimetry; LINCR, lung-inducible Neuralized related C₃HC₄ RING finger protein; NECD, Notch receptor extracellular domain; Neur, Neuralized protein from *Drosophila melanogaster*; NHR, neuralized homology repeat; NICD, Notch receptor intracellular domain; NOE, nuclear Overhauser enhancement; NOESY, NOE spectroscopy; SOCS, Suppressor of Cytokine Signaling.

⁶Laboratory for
Immunogenomics, RIKEN
Research Center for
Allergy and Immunology,
1-7-22 Suehiro-cho,
Tsurumi, Yokohama
230-0045, Japan

⁷Protein Design Laboratory,
Yokohama City University,
1-7-29 Suehiro-cho, Tsurumi,
Yokohama 230-0045, Japan

⁸Department of Biophysics
and Biochemistry,
Graduate School of Science,
The University of Tokyo,
7-3-1 Hongo, Bunkyo-ku,
Tokyo 113-0033, Japan

Received 9 February 2009;
received in revised form
3 August 2009;
accepted 10 August 2009
Available online
14 August 2009

Edited by A. G. Palmer III

Keywords: solution structure; NMR; Neuralized (Neur); neuralized homology repeat (NHR) domain; Notch signaling pathway

Introduction

The Notch pathway is an evolutionarily conserved cell–cell signaling system that plays a critical role in cell-fate decisions throughout development.^{1–3} The Notch receptor is composed of the extracellular domain (NECD) and the intracellular domain (NICD), which are bound to each other noncovalently.⁴ The canonical Notch signaling system is activated when one of the Notch ligands (Delta and Serrate in *Drosophila*, Lag2 in *Caenorhabditis elegans*) in the signal-sending cell binds to the NECD of the Notch receptor in a signal-receiving cell. In *Drosophila*, the intracellular domains of the Notch ligands (Delta and Serrate) must be monoubiquitinated by either the Neuralized protein (Neur) or the *Drosophila* Mind bomb protein (D-mib) to be targeted for endocytosis into the signal-sending cell.^{5–14} Although Neur and D-mib are functionally interchangeable as ubiquitin E3 ligases for Delta, they share no obvious sequence similarity, apart from a canonical RING finger required for their E3 ligase activities.^{15–17} Upon the endocytosis of Delta into the signal-sending cell with the NECD, the NICD of the Notch receptor is released from the membrane and translocated into the nucleus of the signal-receiving cell, where it activates Notch-targeted gene expression (Fig. 1).^{1,2,18–21}

Neur is a peripheral membrane protein composed of 754 amino acid residues. It comprises one C-terminal RING finger and two consecutive neur-

alized homology repeat (NHR) domains, NHR1 and NHR2, which are also referred to as NEUZ domains (Fig. 2a).^{9,24,25} The C-terminal RING finger is responsible for the ubiquitin E3 ligase activity required for the ubiquitination of Delta, as described above. The NHR1 domain is necessary and sufficient for the binding to Delta.²⁶ Mutations in Neur result in a variety of developmental defects that closely resemble those observed in mutants of the Notch ligands and the Notch receptor.^{27–29} These results indicated that Neur plays a critical role in the Notch signaling system and must be tightly controlled in the signal-sending cell in order to ensure the correct pattern of Delta trafficking and signal transduction.

The regulatory proteins from the Bearded protein family, such as Tom, reportedly interact specifically with Neur and block the Neur-mediated endocytosis of Delta, but not the pathway regulated by D-mib (Fig. 1).^{30,31} At least eight *Bearded*-like genes (*m2*, *m4*, *m6*, *m α* , *bob*, *brd*, *tom*, and *ocho*) have been identified in the *Drosophila melanogaster* genome.^{32,33} All of the gene products, except for *m2*, contain the conserved amino acid sequence referred to as motif 2 and interact with Neur. Further deletion and point mutation analyses of Tom demonstrated that motif 2 is critical for Neur binding.³¹ In addition, yeast two-hybrid screening and coimmunoprecipitation experiments demonstrated that the NHR1 domain of Neur (the Neur NHR1 domain) was required

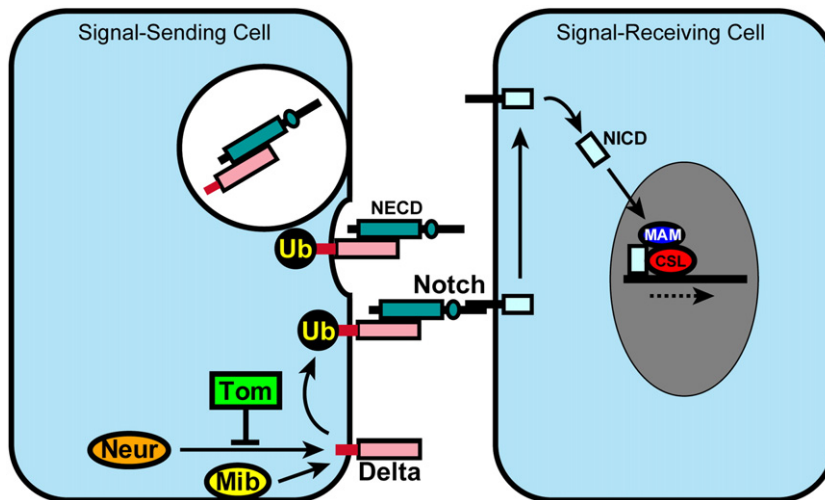


Fig. 1. The Notch signaling pathway in *Drosophila*. The Notch receptor in the signal-receiving cell is composed of the Notch extracellular domain (NECD) and the Notch intracellular domain (NICD). Delta (Notch ligand) is in the signal-sending cell, and its binding to the NECD triggers the endocytosis of Delta with the NECD into the signal-sending cell. The endocytosis activates a cascade of proteolysis of the NICD, and finally the NICD is released from the membrane. Subsequently, the processed NICD enters the nucleus and interacts with the DNA-binding protein, CSL [CBF1, Su(H) and LAG-1]

complex (red). Along with other transcriptional factors, such as the coactivator Mastermind (MAM, blue), the CSL complex activates the transcription of the target gene. The monoubiquitination of Delta is a prerequisite for its endocytosis. Neuralized (Neur, orange) and Mind bomb (Mib, yellow) are the E3 ligases for the monoubiquitination of Delta (Notch ligand). Tom (green) specifically inhibits the ubiquitination of Delta by Neur.

for binding to the 20-residue peptide corresponding to motif 2 of Tom. Therefore, it has been suggested that the NHR domains can function in facilitating protein–protein interactions^{30,31} and that the specific binding of motif 2 of Tom to the Neur NHR1 domain inhibits the interaction between Neur and Delta.

The NHR domain is a novel protein module, and several proteins containing between one and six NHR domains have been found in fly, worm, and mammalian proteins. According to the domain organization, the NHR-domain-containing proteins can be classified into three subfamilies: those including the RING finger (the RING finger subfamily), the Suppressor of Cytokine Signaling box³⁴ (the SOCS box subfamily), and the NHR-only subfamily. The RING finger subfamily proteins contain one or two N-terminal NHR domains and one C-terminal RING finger, such as LINCR (lung-inducible Neuralized related C₃HC₄ RING finger protein), which is an inflammation-induced E3 ligase,³⁵ and Neur.^{5,6,9,10,28,36} The proteins of the SOCS box subfamily contain only one N-terminal NHR domain and one C-terminal SOCS box, such as mouse Neurl2, also referred to as Ozz.^{37,38} Ozz is a muscle-specific E3 ligase regulating β -catenin proteasomal degradation during myogenesis.^{37,38} The SOCS box in Ozz functions as an adaptor of the E3 ligase complex, composed of Cullin-5, Elongin B/C, and Rbx1.^{38,39} Therefore, the members of the RING finger and SOCS box subfamilies are all ubiquitin E3 ligases, and the NHR domains in these subfamilies are thought to mediate the specific protein–protein interactions for the recognition of the substrates for ubiquitination. On the other hand, the proteins from the NHR-only subfamily, which contain six NHR domains and are exemplified by the human KIAA1787 protein, have not been well characterized thus far (Fig. 2a).

To gain more structural insight into the regulation of the Notch signaling pathway by the NHR

domains, we have determined the solution structure of the Neur NHR1 domain and investigated the interaction between the NHR1 domain and a 20-residue peptide derived from motif 2 of Tom. In addition, in order to examine the commonalities and the differences among the NHR domains, we also solved the structure of the first NHR domain of the human KIAA1787 protein (the KIAA1787 NHR1 domain) from the NHR-only subfamily, whose members are not E3 ligases. On the basis of these data, we discuss the interaction mode of the Neur NHR1 domain from a structural point of view.

Results and Discussion

Identification of the domain boundaries of the NHR domain

We first tried to identify the domain boundaries of the Neur NHR1 domain to conduct a structural analysis of this novel domain. On the basis of the sequence alignment from various databases, (Pfam[†], SMART[‡], and Uniprot[§]), the NHR domain is defined by nearly 60, 120, and 160 amino acid residues, respectively. Among these databases, the definitions of the N-terminal end of the NHR domains were almost the same, but those of the C-terminal end were different from each other. This is probably caused by the fact that high level of homology is observed among the N-terminal portions of the NHR domains, but low level of

[†] <http://pfam.sanger.ac.uk/>

[‡] <http://smart.embl-heidelberg.de/smart/>

[§] <http://www.uniprot.org/>

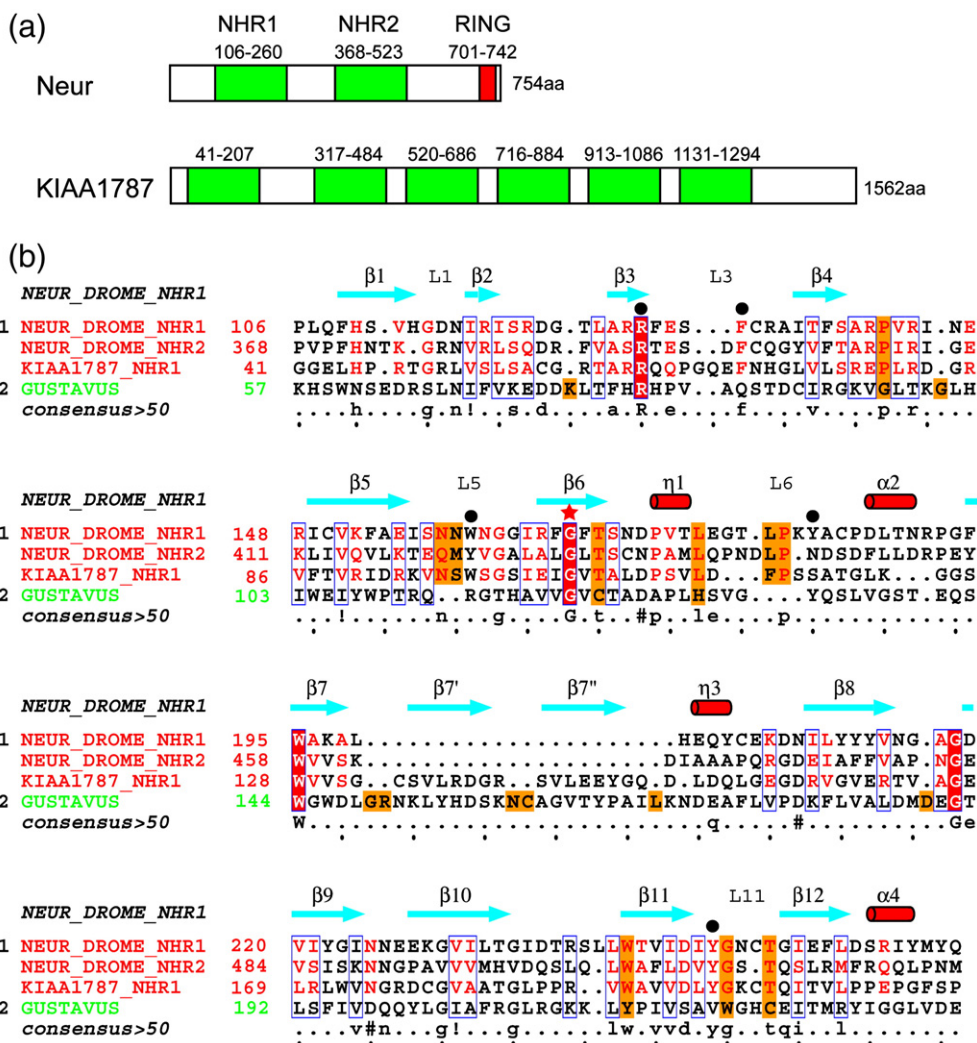


Fig. 2. Domain architectures and sequence alignment of the Neur and human KIAA1787 proteins. (a) Domain architectures of Neur and human KIAA1787 proteins are shown with the NHR domains (green) and RING finger (red). The boundaries of the NHR domains and the RING finger are indicated on the basis of information from the Uniprot database (<http://www.ebi.ac.uk/uniprot/>). (b) Structure-based sequence alignment of the NHR1 and NHR2 domains of Neur, the NHR1 domain of KIAA1787, and the B30.2/SPRY domain of GUSTAVUS.²² The red star indicates the only absolutely conserved residue (Gly) in the NHR domains. The filled circles indicate the conserved, but solvent-exposed, residues at the bottom area of the β -sandwich fold. Secondary-structure elements of the Neur NHR1 domain are depicted above the aligned sequences. The sequence alignment output was created with the ESPript program.²³

homology is found among the C-terminal ones. Therefore, as described in the [Materials and Methods](#), we examined several constructs with around 60, 120, and 160 amino acid residues, using green fluorescent protein (GFP) as a C-terminal fusion^{40,41} in a batch mode with our cell-free protein synthesis system.^{42,43} At the same time, we tried to identify the

domain boundaries by monitoring the soluble fractions by SDS-PAGE experiments (see [Materials and Methods](#)). We thus successfully identified several constructs for the soluble Neur NHR1 domain, which were composed of around 160 amino acid residues (spanning residues 96–266, 96–276, 106–266, and 106–276) (Fig. S1). Lastly, with the

Fig. 3. 2D ^1H - ^{15}N HSQC spectrum and ITC data of the Neur NHR1 domain. (a) 2D ^1H - ^{15}N HSQC spectrum of the Neur NHR1 domain, recorded at the ^1H frequency of 800 MHz, pH 7.0, and 298 K. Cross-peaks are labeled with the residue numbers. Side-chain resonances of asparagine and glutamine residues are indicated by horizontal lines. ITC data for the interaction of the wild-type Neur NHR1 domain (b) and the mutant Neur NHR1 domain (Y183S) (c) with the 20-residue Tom peptide. Top: the exothermic heat reaction, measured with the injection of the 20-residue Tom peptide into the protein samples. Bottom: plot of the total heat released as a function of the molar ratio of the 20-residue Tom peptide. The continuous line represents the nonlinear, least-squares best fit to the experimental data using a one-site model.

uniformly ^{15}N -labeled samples of these soluble constructs, we measured the two-dimensional (2D) ^1H - ^{15}N heteronuclear single-quantum coherence (HSQC) spectra. We then determined that the segment spanning residues 106–266 of the Neur protein yielded a well-resolved spectrum (Fig. 3a) and that the construct was properly folded as the minimum Neur NHR1 domain.

We investigated the physical interactions between the Neur NHR1 domain identified here and a 20-residue peptide derived from motif 2 of Tom by isothermal titration calorimetry (ITC) experiments (Fig. 3b). The ITC experiments revealed the distinct binding between the Neur NHR1 domain and the 20-residue peptide with a binding constant $K_d=2.53\pm 0.024\ \mu\text{M}$ (Fig. 3b). The molar ratio from the ITC experiments indicated that the Neur NHR1 domain forms a one-to-one complex with the Tom peptide. Therefore, we concluded that this construct, with 161 amino acid residues (Pro106–Gln266) of the Neur NHR1 domain, is not only structured but also functional. In the following discussion, the residues are numbered as shown in the first line of Fig. 2b. Similarly, the human KIAA1787 NHR1 domain, spanning residues Glu43–Leu205, was also identified for the structure determination. The $^{15}\text{N}/^{13}\text{C}$ -labeled samples of both NHR domains were prepared by a large-scale cell-free protein synthesis system^{42,43} for solution structure determination by NMR.

Resonance assignments and NMR structure determination

Using a combination of triple-resonance NMR experiments, we performed chemical shift assignments for the Neur NHR1 domain and the KIAA1787 NHR1 domain by standard methods, (see Materials and Methods). In the case of the Neur NHR1 domain, the backbone and side-chain resonance assignments were complete, except for the amide protons of Arg121, Arg122, and Gly123 as well as H^α of Arg121, the side chain of Arg122, H^β of Arg165, and H^ϵ of Phe129 and Phe132. The side-chain NH_2 resonances of all Asn and Gln residues were assigned. The assignments were confirmed by tracing the d_{NN} , $d_{\alpha\text{N}}$, and $d_{\beta\text{N}}$ connectivities in nuclear Overhauser enhancement (NOE) spectroscopy (NOESY) experiments.⁴⁴ Inspection of the $\text{X}(\text{H}^\alpha)\text{--Pro}(\text{H}^\beta)$ sequential NOESY cross-peaks and the $^{13}\text{C}^\beta/^{13}\text{C}^\gamma$ chemical shift differences⁴⁵ revealed that all of the X-Pro peptide bonds in the Neur NHR1 domain, except for Pro186, are in the trans conformation.

The total of 5388 cross-peaks identified in the ^{15}N - and ^{13}C -edited 3D NOESY spectra resulted in 2984 nonredundant distance restraints, including 1209 long-range distance restraints, for the final structure calculations with the program CYANA 2.1.^{46,47} Backbone torsion angle restraints calculated by the TALOS program⁴⁸ and hydrogen bonds derived from the NOE network were incorporated in the final stage of the structure calculation. The final structures were further refined by minimization with

AMBER9||. The precision of the bundle of 20 conformers that represents the solution structure of the Neur NHR1 domain is characterized by RMSD values to the mean coordinates for residues 106–265 of 0.50 Å for the backbone atoms and 1.04 Å for all heavy atoms (Fig. 4a). The quality of the structure is also reflected by the fact that 97.9% of the (ϕ, ψ) backbone torsion angle pairs are in the most favored and additionally allowed regions of the Ramachandran plot, according to the program PROCHECK-NMR.⁴⁹

The chemical shift assignments and the structure calculation for the KIAA1787 NHR1 domain were performed in the same way. The backbone and side-chain resonance assignments were complete, except for the amide protons of Arg85, Ala91, Cys92, and Arg94, and H^ϵ of Phe105 and Phe151. All side-chain NH_2 resonances of the Asn and Gln residues were assigned, and all X-Pro peptide bonds were in the trans conformation. The total of 7018 cross peaks identified in the ^{15}N - and ^{13}C -edited 3D NOESY spectra resulted in 4011 nonredundant distance restraints, including 1753 long-range distance restraints, and the solution structure of the KIAA1787 NHR1 domain was calculated using the same protocol as described above. The precision of the structure is characterized by RMSD values to the mean coordinates for residues 43–205 of 0.25 Å for the backbone atoms and 0.70 Å for all heavy atoms (Fig. 4c).

The solution structures of the NHR1 domains of Neur and KIAA1787 are well defined and in excellent agreement with the experimental NMR restraints. Statistics regarding the quality and precision of the final 20 best conformers that represent the solution structures of the Neur NHR1 domain (Fig. 4a and b) and the KIAA1787 NHR1 domain (Fig. 4c and d) are provided in Table 1. Due to the poor stability and solubility of the Neur NHR1 sample, the qualities of the 3D NOESY spectra of the Neur NHR1 domain were worse than those for the KIAA1787 NHR1 domain. Accordingly, the statistics of the 3D structures of the KIAA1787 NHR1 domain are better than those of the Neur NHR1 domain.

Solution structures of the two types of NHR domains

The Neur NHR1 domain contains 12 β -strands (β 1: Phe109–His113; β 2: Ile117–Ile119; β 3: Ala126–Arg128; β 4: Ile136–Ser139; β 5: Ile149–Glu155; β 6: Arg165–Thr169; β 7: Phe194–Ala198; β 8: Ile209–Val214; β 9: Asp219–Ile224; β 10: Glu228–The234; β 11: Trp243–Asp247; and β 12: Gly254–Leu258). These β -strands constitute a two-layered β -sandwich fold, composed of five-stranded (β 1– β 4– β 11– β 6– β 7) and seven-stranded (β 2– β 3– β 12– β 5– β 8– β 9– β 10) antiparallel β -sheets (Fig. 4a and b). The β -strands are connected by loops with various lengths (L1–L11), which extend out from both ends of the β -sandwich.

|| <http://amber.scripps.edu>

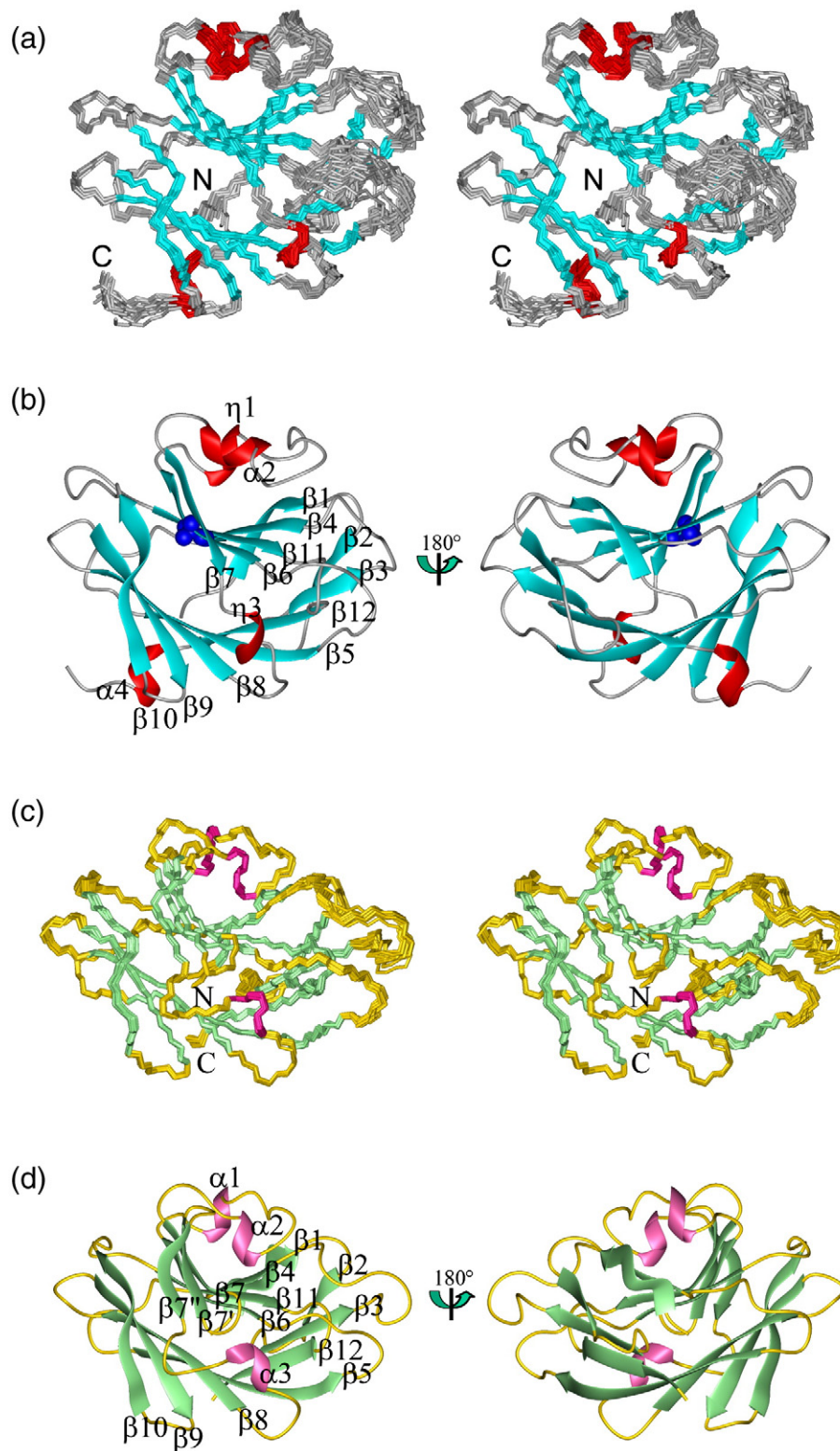


Fig. 4. Overall structures of the NHR1 domains of Neur and human KIAA1787. (a) Stereo view of the ensemble of 20 structures that represents the solution structure of the Neur NHR1 domain (residues 106–266). The N- and C-termini are indicated by the letters N and C. (b) Ribbon representation of the Neur NHR1 domain. The α -helices, β -sheets, and loop regions are depicted in red, cyan, and gray, respectively, and the secondary structure components are labeled by Greek letters. The atoms of G167 are also indicated as blue spheres. The view on the right is rotated by 180° around the z-axis from that on the left. (c) Stereo view of the ensemble of 20 structures that represents the solution structure of the KIAA1787 NHR1 domain (residues 43–205). (d) Ribbon representation of the KIAA1787 NHR1 domain, with the secondary structure components labeled. The α -helices, β -sheets, and loop regions are depicted in hot pink, pale green, and gold, respectively. The view on the right is rotated by 180° around the z-axis from that on the left.

Table 1. Structural statistics for the NHR1 domains of Neur and KIAA1787

	Neur	KIAA1787
<i>Conformational restraints</i>		
NOE distance restraints		
Total	2984	4011
Intraresidue	707	774
Sequential ($ i-j =1$)	729	1025
Medium range ($1 < i-j < 5$)	339	459
Long range ($ i-j \geq 5$)	1209	1753
ϕ/ψ dihedral angle restraints from TALOS ⁴⁸	73/73	79/79
Restrained hydrogen bonds	21	9
<i>Structure statistics</i>		
CYANA target function (\AA^2)	0.65	0.50
Residual NOE violations		
Number $>0.10 \text{\AA}$	1	1
Maximum (\AA)	0.22	0.12
Residual dihedral angle violations		
Number $>2.5^\circ$	0	0
Maximum ($^\circ$)	1.10	1.24
Energies (kcal/mol)		
Mean constraint violation energy	13.62	24.46
Mean Amber energy	-5196.82	-5597.79
Ramachandran plot statistics (%) ⁴⁹		
Residues in most favored regions	81.9	87.3
Residues in additional allowed regions	16.0	11.1
Residues in generously allowed regions	1.6	1.5
Residues in disallowed regions	0.5	0.1
RMSD to mean coordinates (\AA)		
Backbone	0.50	0.25
Heavy atoms	1.04	0.70

Ramachandran plot statistics and RMSD values are for residues 106–265 of the Neur NHR1 domain and for residues 43–205 of the KIAA1787 NHR1 domain.

There are four short helices in the loop regions: helix 3_{10} -1 (Pro173–Thr175) and helix α 2 (Asp187–Asn190) in the L6 loop, helix 3_{10} -3 (Glu201–Tyr203) in the L7 loop, and helix α 4 (Ser260–Tyr263) in the C-terminal segment.

Each of the two β -sheets forms a central flat and elongated hydrophobic patch on the outer surface of the protein. The L6 loop (Ser170–Gly193) is composed of 24 amino acid residues and adopts a characteristic structure covering the concave surface of the five-stranded β -sheet, to protect the hydrophobic patch and to increase the globular nature of the molecule. Similarly, the C-terminal segment containing the α 4 helix is folded onto the convex surface of the seven-stranded β -sheet, where it covers the hydrophobic patch.

Furthermore, we also determined the tertiary structure of the human KIAA1878 NHR1 domain. This domain contains 14 β -strands (β 1: Leu44–Thr48; β 2: Val52–Leu54; β 3: Thr60–Arg63; β 4: Val75–Leu76; β 5: Val86–Lys94; β 6: Glu103–Thr107; β 7: Ser127–Val130; β 7': Ser134–Arg137; β 7'': Ser141–Glu144; β 8: Arg158–Arg163; β 9: Glu133–Val173; β 10: Asp177–Thr183; β 11: Trp190–Asp194; and β 12: Cys199–Val204) and forms a two-layered β -sandwich fold similar to that of the Neur NHR1 domain (Fig. 4c and d). However, the upper layer of the concave β -sheet is a seven-stranded antiparallel

β -sheet with a β 1– β 4– β 11– β 6– β 7– β 7'– β 7'' topology (Figs. 4c and d and 5a and b). The peptide segment corresponding to the L7 loop of the Neur NHR1 domain is longer in the KIAA1787 NHR1 domain, and it forms an additional β -hairpin structure (β 7'– β 7'') that associates with the β 7' strand of the upper β -sheet. There are three short helices in the loop regions: helix 3_{10} -1 (Pro111–Val113) and helix 3_{10} -2 (Ala120–Gly122) in the L6 loop, and helix 3_{10} -3 (Leu150–Glu152) in the L7 loop (Fig. 4d).

Similar to the Neur NHR1 domain, the KIAA1787 NHR1 domain possesses a hydrophobic patch on the upper β -sheet, and the L6 loop in the KIAA1787 NHR1 domain contains two helical structures that cover this hydrophobic area. In the case of the KIAA1787 NHR1 domain, relatively hydrophilic amino acids are located at the central two β -strands (β 5 and β 12) of the lower β -sheet, as compared to the Neur NHR1 domain (Fig. 2b). Correspondingly, the KIAA1787 NHR1 domain is soluble and stable, even without the C-terminal short α -helix that covers the hydrophobic patch on the lower β -sheet surface in the Neur NHR1 domain (Fig. 4b and d).

Structural comparison between the two NHR domains

The NHR1 domains of Neur and KIAA1878 share 28% sequence identity. The superposition of the two structures shows close agreement (RMSD 2.1 \AA) with the same β -sandwich fold, except for the above-mentioned additional β -hairpin in the KIAA1787 NHR1 domain (Fig. 5a and b). Further examination of the locations of the hydrophobic amino acids highlighted the common and distinct features between the two NHR1 domains.

The hydrophobic amino acids that constitute the area in between the two β -sheets in the NHR1 domains of Neur and KIAA1787 are well conserved, even among the NHR domain family (Fig. S2). Overall, the amino acids are particularly well conserved in the region spanning the N-terminal 60 residues, after which the total amino acid conservation becomes poor. Nevertheless, similarities of the key hydrophobic amino acid residues that are involved in forming the structure are observed throughout the sequences (Fig. S2).

Both of the NHR1 domains possess a hydrophobic patch on the upper β -sheet, and the long L6 regions cover this hydrophobic area. Two helical structures are conserved in the L6 regions, as described above (Fig. 4b and d). Pro173, Leu180, Pro181, and Leu188 of the Neur NHR1 domain, which are located in the region from the 3_{10} -1 helix to the α 2 helix in the L6 loop, are well conserved, and an alkyl hydrophobic amino acid occupies the position corresponding to Leu176 of the Neur NHR1 domain in most of the NHR domain family members (Fig. 2b and Fig. S2). These hydrophobic amino acid residues in the L6 loop interact with those on the upper β -sheet by van der Waals contacts in these two NHR domain structures. Therefore, we consider the characteristic L6 loop structure of the NHR1 domains of Neur and

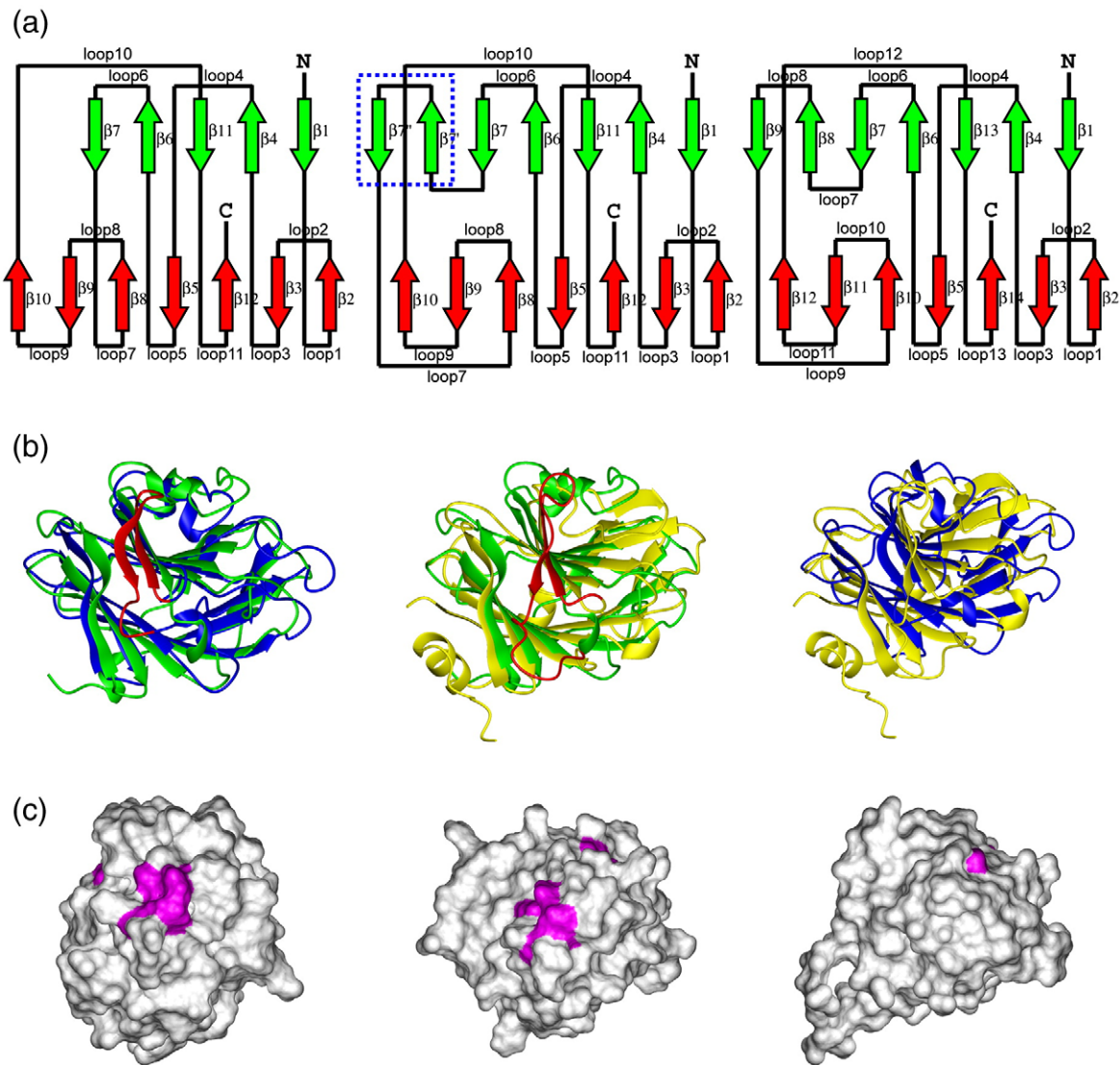


Fig. 5. Comparison of the structural homologues among the NHR1 domains of Neur and KIAA1787, and B30.2/SPRY of GUSTAVUS²² (PDB entry 2IHS). (a) The topology of the Neur NHR1 domain (left), KIAA1787 NHR1 domain (middle), and the B30.2/SPRY domain of GUSTAVUS (right) are demonstrated, respectively. (b) Left: pairwise superposition of the ribbon structures of the NHR1 domains of Neur (green) and KIAA1787 (blue). Middle: pairwise superposition of the ribbon structures of the NHR1 domain of Neur (green) and the B30.2/SPRY domain of GUSTAVUS²² (yellow). Right: pairwise superposition of the ribbon structures of the NHR1 domain of KIAA1787 (blue) and the B30.2/SPRY domain of GUSTAVUS (yellow). In the superpositions, the additional β -hairpin structures in the NHR1 domain of KIAA1787 (left) and the B30.2/SPRY domain of GUSTAVUS²² (middle) are colored red. (c) Left: surface representation of the Neur NHR1 domain with the conserved aromatic residues between the NHR1 domains of the Neur and KIAA1787 proteins. Middle: the conserved aromatic residues between the NHR1 domains of the Neur and KIAA1787 proteins on the surface representation of the KIAA1787 NHR1 domain. Right: surface representation of the B30.2/SPRY domain of GUSTAVUS (right). In the surface representations, the aromatic residues, which are conserved at the corresponding positions in the NHR1 domains of Neur and KIAA1787 protein based on the sequence alignment of Fig. 2b, are colored magenta. The conserved and exposed aromatic amino acids are depicted on the surface model. The orientations of the ribbon structures and the surface representations are the same as in the left diagram and after a -70° rotation on the y -axis from the left diagram in Fig. 4b, respectively.

KIAA1787 to be a common feature of the NHR domain family. A previous report indicated that the G167E mutation of the Neur NHR1 domain critically affected the Neur activity.²⁶ The Gly167 residue, which is the only absolutely conserved residue among the NHR domains, is located at the center of the β_6 strand in the Neur NHR1 domain (Fig. 4b), and the space above Gly167 is occupied by

hydrophobic amino acid residues from the L6 loop. Accordingly, Gly167 has a total of 24 NOEs with the amino acid residues in the hydrophobic core, including those from the L6 loop. Presumably, any mutation of the Gly167 residue fills the space and alters the arrangement of the other residues in the hydrophobic core, thus destabilizing the β -sandwich fold.

The hydrophobic amino acid residues that sustain the structure of the NHR domains are well conserved, as described above. On the other hand, when we highlighted all of the conserved aromatic amino acids among these NHR domains, we could identify those (Phe132, Trp160, and Tyr249) residing on the molecular surface. They are located at the bottom area of the β -sandwich, and could access the solvent (Fig. 5c). Arg128, which is proximal to these aromatic amino acid residues, is also conserved in the NHR domain family. On the contrary, Tyr183, at the tip of the L6 loop, is a unique hydrophobic residue in the Neur NHR1 domain, among the NHR domain family members (Fig. 2b and Fig. S2). These amino acid residues could participate in specific target binding, and will be discussed below.

The NHR domain subfamilies

As introduced above, the NHR-domain-containing proteins can be classified into the RING finger, SOCS box, and NHR-only subfamilies (Fig. S2). The proteins from these three subfamilies are exemplified by Neur or LINCR,³⁵ Ozz,^{37,38} and the human KIAA1787 protein, respectively. A phylogenetic tree analysis of the NHR domains, on the basis of the domain boundaries with around 160 amino acid residues, is consistent with the subfamilies classified according to the domain organization of the NHR-domain-containing proteins (Fig. 6).

The regions corresponding to the L6 and L7 loops vary in length and amino acid composition among

the NHR subfamilies. The hydrophobic amino acids that are conserved in the L6 loop in the NHR1 domains of Neur and KIAA1787 are also present in the SOCS box subfamily. Thus, it is probable that the L6 loops for all of the NHR subfamilies adopt similar structures. A sequence alignment of the NHR domains of the SOCS box subfamily indicates that a seven-residue segment preceding the α 2 helix, which could be located at the tip of the L6 loop, is highly conserved within the subfamily. In the case of the Neur NHR1 domain, this region plays an important role in the recognition of the specific target, as described below. Thus, the sequence conservation observed in the SOCS box subfamily seems to be important for the specific target recognition by the subfamily members.

The L7 loop of the RING finger subfamily is shorter than those in the SOCS box and NHR-only subfamilies (Fig. S2). From the sequence alignment and the present solution structures, the NHR domains of the RING finger subfamily are expected to have a five-stranded upper β -sheet, whereas the NHR domains of the NHR-only subfamily have a seven-stranded upper β -sheet. Like the NHR-only subfamily, the SOCS box subfamily also has the long L7 loop. However, for the KIAA1787 NHR1 domain of the NHR-only subfamily, the characteristic hydrophobic amino acids, Val135 on the β 7' strand, Val142 on the β 7'' strand, and Tyr146 in the loop region just after the β 7'' strand, are well conserved and seem to be necessary for the formation of the additional β -hairpin structure. Instead, in the SOCS

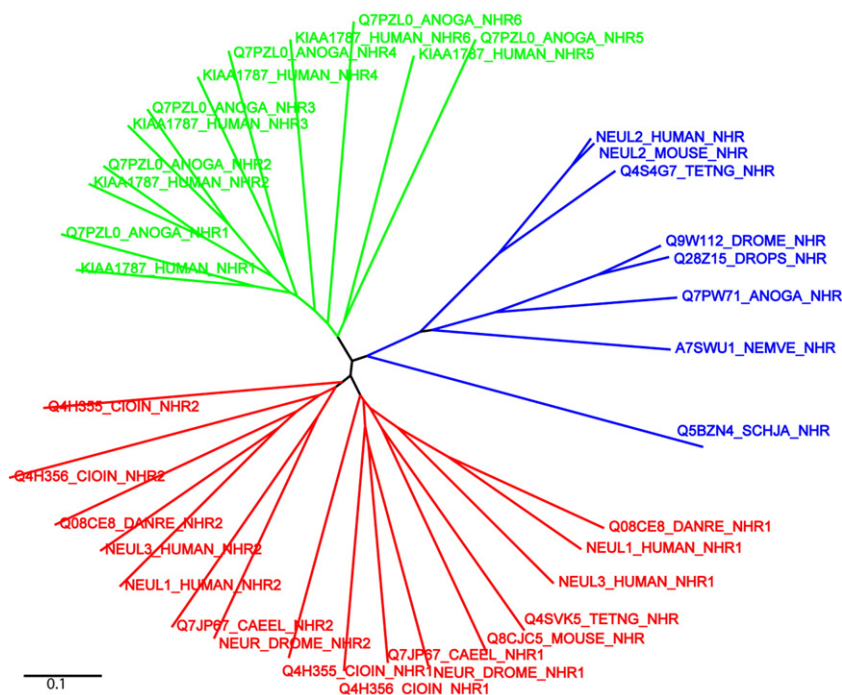


Fig. 6. An unrooted phylogenetic tree of the NHR domain family. The scale bar indicates the number of substitutions per site. Note that the NHR domains are classified into three subfamilies: the RING finger, SOCS box, and NHR-only subfamilies, shown in red, green, and blue, respectively. The domains are labeled with the protein accession codes, followed by the corresponding species names and the domain position numbers.

box subfamily, such hydrophobic amino acids are missing, and relatively hydrophilic amino acids are located in the region corresponding to the $\beta 7'$ strand. Thus, it is probable that the region corresponding to the $\beta 7'$ - $\beta 7''$ hairpin in the NHR-only subfamily adopts a unique structure in the SOCS box subfamily, although no structure for the NHR domain of this subfamily has been reported yet.

Tertiary structure comparison with the B30.2/SPRY domain

A structural similarity search was performed with the program Dali,⁵⁰ using the solution structure of the Neur NHR1 domain as the query structure. The NHR1 domain structure of the human KIAA1787 protein [Protein Data Bank (PDB) entry 2E63] was retrieved with the highest Z-score (16.9) and smallest RMSD value (2.1 Å), although it contains two additional antiparallel β -strands ($\beta 7'$ - $\beta 7''$) within the β -sandwich fold, as described above (Figs. 4c and d and 5a and b).

The other candidates from the Dali⁵⁰ search with high Z-scores (>10) are B30.2/SPRY domain structures, such as GUSTAVUS (PDB entries 2FNJ,⁵¹ 2IHS²²), the B30.2/SPRY-domain-containing SOCS box proteins 1, 2, 3, and 4 (PDB entries 2JK9, 3EK9,⁵² 2YYO, and 2V24, respectively), the similar to ret finger-protein-like 1 (PDB entry 2FBE⁵³), and murine Trim21 (PDB entries 2VOL,⁵⁴ 2VOK,⁵⁴ and 2IWG). The B30.2/SPRY domains are known to mediate protein-protein interactions. Interestingly, the B30.2/SPRY domain is also found associated with the SOCS box in negative regulators of cytokine signaling,⁵⁵ and this domain has been shown to mediate the interactions between the hepatocyte growth factor receptor, MET, and adaptor proteins.^{56,57}

We chose the B30.2/SPRY domain of GUSTAVUS²² (PDB entry 2IHS) as an example for a comparison with the structures of the two NHR domains obtained in this study. Pairwise superpositions of the Neur NHR1 domain, the KIAA1787 NHR1 domain, and the B30.2/SPRY domain of GUSTAVUS are shown in Fig. 5b. The KIAA1787 NHR1 domain and the B30.2/SPRY domain of GUSTAVUS share the same topology and very similar 3D structures (RMSD 3.0 Å), in spite of the low level of sequence identity of about 10% (Fig. 5a and b). The positions of the key hydrophobic amino acids that play important roles in the formation of the β -sandwich structure are occupied by similar or identical hydrophobic amino acids between the NHR domains and the B30.2/SPRY domain (Fig. 2b). On the other hand, when we highlighted the conserved aromatic amino acids between the Neur NHR1 domain and the B30.2/SPRY domain, it revealed that the region containing the exposed, but well conserved, aromatic amino acids among the NHR domains was absent in the B30.2/SPRY domain (Fig. 5c). This region is involved in the target-binding site, and the structural differences will be discussed below.

Interactions between the NHR1 domains and the Tom peptide

The members of the Bearded protein family have been reported to interact with Neur through the NHR1 domain.³¹ The interactions between the Neur NHR1 domain and a 20-residue peptide derived from motif 2 of Tom, a Bearded protein family member, were investigated by NMR spectroscopy. We performed titration experiments with the peptide and the uniformly ¹⁵N/¹³C-labeled Neur NHR1 domain, in which the binding was monitored by tracing the backbone amide signals.

The backbone amide peaks did not change continuously, but new resonances appeared when the peptide-protein ratio was increased from 0.2:1 to 0.5:1. The distinct signals for the free and bound states indicated that the dynamics of the binding between the Neur NHR1 domain and the Tom peptide is in the slow exchange regime, and that the binding affinity is relatively strong (the overlaid spectra of the free and bound (1:1) states are shown in Fig. 7). The interaction with a micromolar dissociation constant ($K_d=2.53\pm 0.024 \mu\text{M}$) was confirmed by the ITC experiments (Fig. 3b). The backbone amide chemical shift perturbations (Fig. 8a) were mapped on the solution structure of the Neur NHR1 domain (Fig. 8b and c). The region affected by the peptide binding is concentrated at the bottom area of the β -sandwich and is composed of the L3, L5, and L11 loops as well as the tip of the L6 loop (Fig. 8b and c). Therefore, this region is directly involved in the interaction with the Tom peptide and/or the structural changes are induced within this region upon binding to the Tom peptide.

On the contrary, the addition of the 20-residue peptide to the KIAA1787 NHR1 domain did not cause significant chemical shift changes in the 2D ¹H-¹⁵N HSQC spectra (data not shown). A comparison of the two NHR1 domains revealed that the Tyr183 residue on the L6 loop of the Neur NHR1 domain is replaced by an amino acid with a small side chain (Ser119) in the KIAA1787 NHR1 domain (Fig. 2b), whereas the aromatic amino acids (corresponding to Phe132, Trp160, and Tyr249 in the Neur NHR1 domain) that are located on the L3, L5, and L11 loops are conserved between these two NHR domains (Fig. 2b). Due to this change, the putative binding pocket that was observed in the Neur NHR1 domain could not be found on the surface of the KIAA1787 NHR1 domain (Fig. 9a and b). In fact, a detailed comparison of the binding interfaces between the two NHR domains revealed that many other chemical properties (charge, hydrophobicity, etc.) also differ between them. The formation of the binding pocket due to the L6 loop thus appears to be an important factor to distinguish the binding activities of the NHR1 domains of Neur and KIAA1787.

Moreover, the Neur NHR2 domain (the second NHR domain of Neur) reportedly did not bind to the Tom peptide,³¹ although it shares 27% sequence

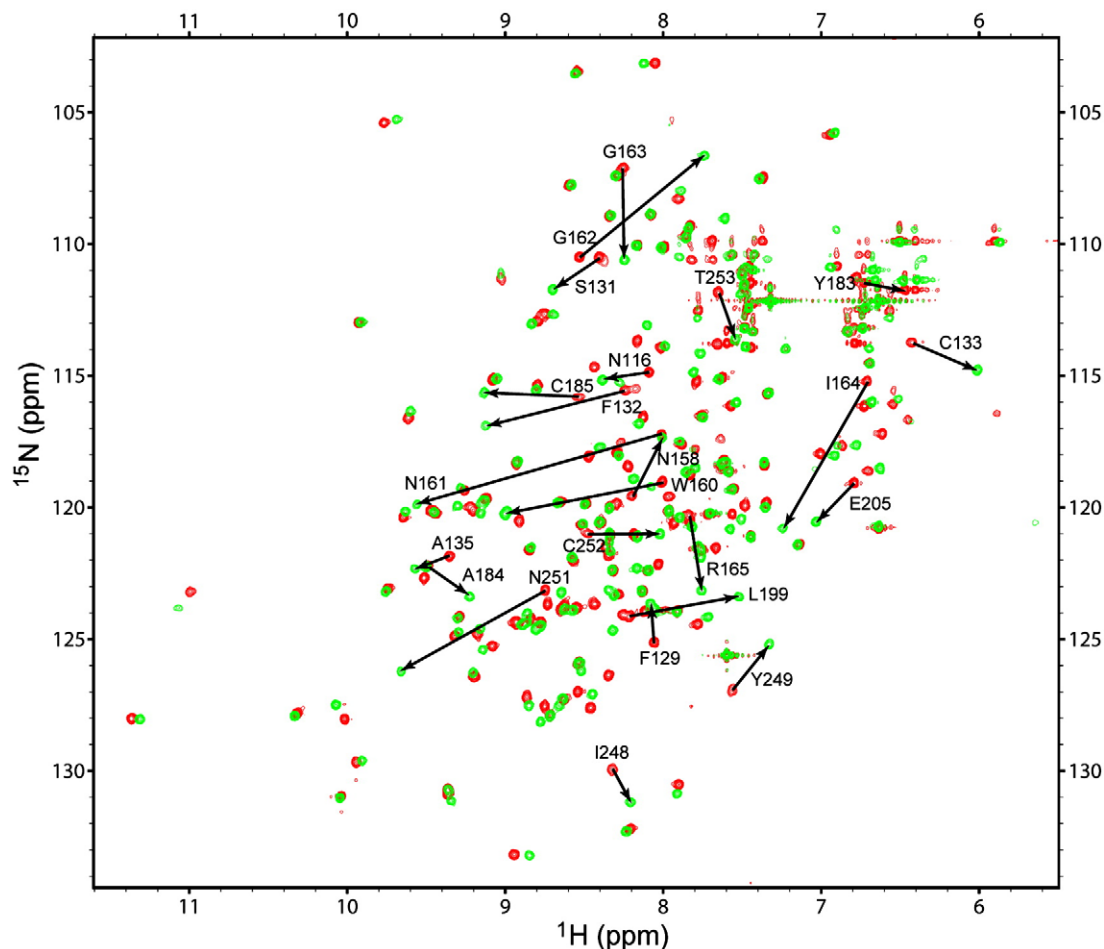


Fig. 7. 2D ^1H - ^{15}N HSQC spectra at a ^1H frequency of 800 MHz of the Neur NHR1 domain, with and without the 20-residue peptide (AASCDNMANEELEQRLYTDL) corresponding to motif 2 of Tom (residues 72–91). The superposition of two ^1H - ^{15}N HSQC spectra at relative molar ratios of the 20-residue Tom peptide to the Neur NHR1 domain of 0:1 (red) and 1:1 (green) is shown. The resonances with significant chemical shift changes upon binding to the 20-residue Tom peptide are labeled by their residue numbers, and the changes in those resonances are marked by arrows.

identity with the adjacent NHR1 domain. Except for the residue corresponding to Tyr183, at the tip of L6 in the Neur NHR1 domain, the other residues in the binding interface are well conserved in the Neur NHR2 domain. Similar to the KIAA1787 NHR1 domain, the Neur NHR2 domain has a hydrophilic amino acid residue (Asn446) at the position corresponding to Tyr183 in the Neur NHR1 domain (Fig. 2b). This comparison again suggests that Tyr183 of the Neur NHR1 domain is the key residue to distinguish the target peptide.

To test this hypothesis, we performed an ITC experiment for the mutant Neur NHR1 domain (Y183S) with the 20-residue Tom peptide. The result revealed only a small change in the heat, in contrast to that of the wild-type Neur NHR1 domain (Fig. 3b and c). This indicated that the mutant Neur NHR1 domain (Y183S) had very little binding activity to the 20-residue Tom peptide. This experiment demonstrated that the Tyr183 residue in the Neur NHR1 domain played a quite critical role for the binding activity and specificity to its target, Tom.

Interaction between the NHR1 domains and the VASA peptide

The B30.2/SPRY domain from GUSTAVUS forms a complex with the peptide from the VASA protein²² (PDB entry 2IHS). Two other complex structures of B30.2/SPRY domains with their ligand peptides are also available in the PDB database: The SPRY domain and SOCS-box-containing protein 1 (SPSB1) in complex with a Par-4 peptide (PDB entry 2JK9) and the human SPRY domain and SOCS-box containing protein 2 (SPSB2) in complex with a 20-residue VASA peptide (PDB entry 3EMW). All of these B30.2/SPRY domains recognize the target peptides with the consensus sequence DINNNN. Actually, Woo *et al.* reported that the six-residue peptide is sufficient for high affinity binding to the B30.2/SPRY domains.²² The binding site on the B30.2/SPRY domain, located at the bottom area of the β -sandwich fold, that is, the L3, L5, and L13 loops, and the tip of the L6 loop are responsible for the interactions (PDB entries 2IHS,²² 2JK9, and 3EMW). The Neur NHR1 domain binds the Tom

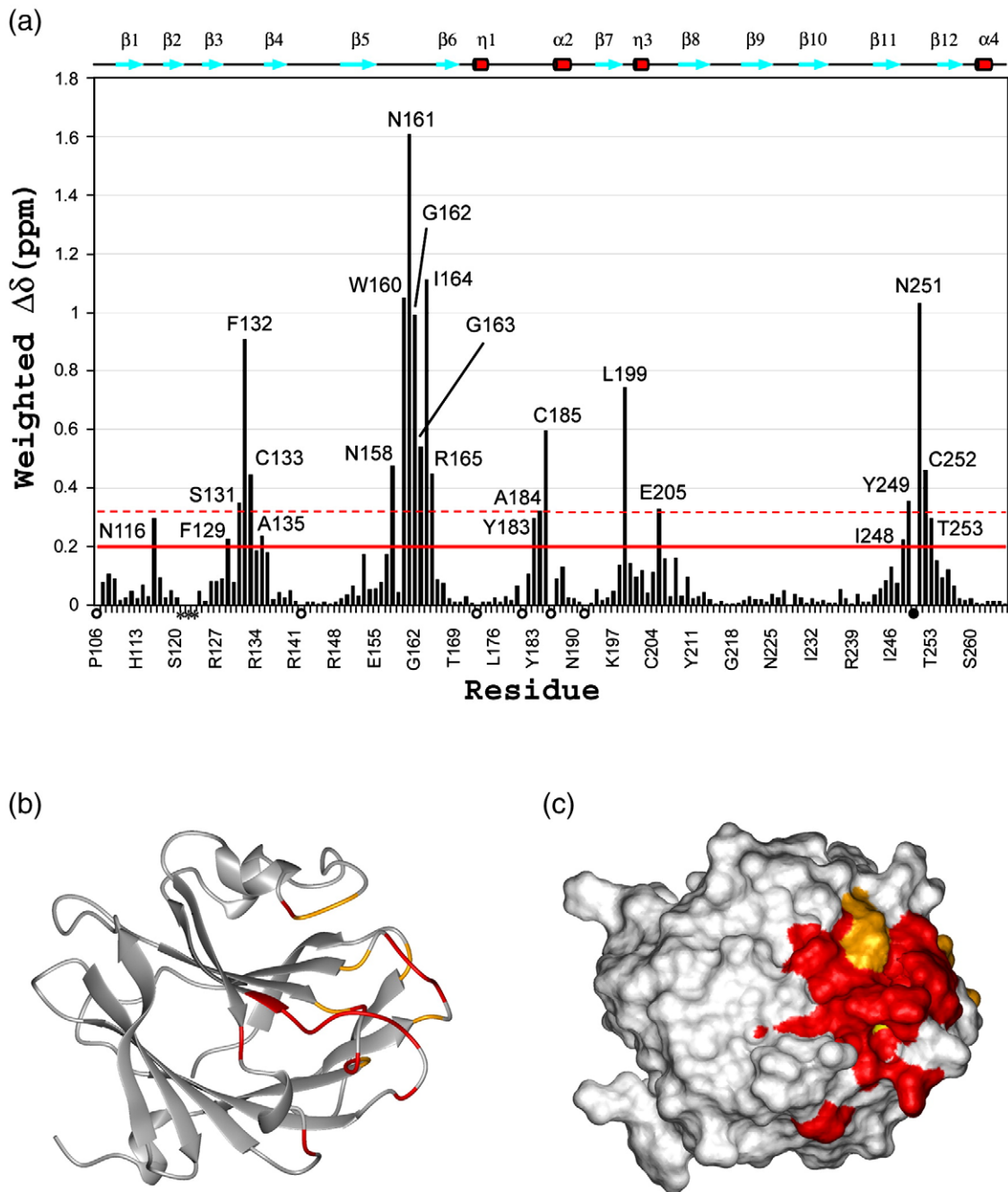


Fig. 8. Results of the NMR titration experiments for the Neur NHR1 domain with the 20-residue Tom peptide. (a) Chemical shift changes obtained from NMR titration experiments, plotted as a function of the residue number. The weighted backbone amide chemical shift changes, $\Delta\delta$, were calculated according to the equation $\Delta\delta = [(\Delta H_N)^2 + (\Delta N/6.5)^2]^{1/2}$.⁵⁸ The residue (G250) missing during the titration is marked with a filled circle below the x -axis. The originally unassigned residues and the proline residues are marked with asterisks and open circles below the x -axis, respectively. The secondary-structure elements are shown at the top. The data of the weighted chemical shift changes are mapped onto a ribbon diagram (b) and the surface (c) of the Neur NHR1 domain. Resonances with weighted backbone amide chemical shift changes above the mean value [continuous red line in (a)] are colored orange, and those with chemical shift changes above the mean value plus one standard deviation [dashed red line in (a)] are colored red.

peptide in a similar location, as described above (Fig. 8b and c). Therefore, we tested whether the NHR1 domains of Neur and KIAA1787 bind to the consensus peptide of the ligand for these B30.2/SPRY domains. However, NMR titration experiments demonstrated that the NHR1 domains of

Neur and KIAA1787 did not bind to the eight-residue peptide (DDINNNNN) derived from the VASA protein (data not shown).

In the case of the B30.2/SPRY domain of GUSTAVUS,²² Trp221, located on the L13 loop, and Tyr133, on the L6 loop, constitute the binding

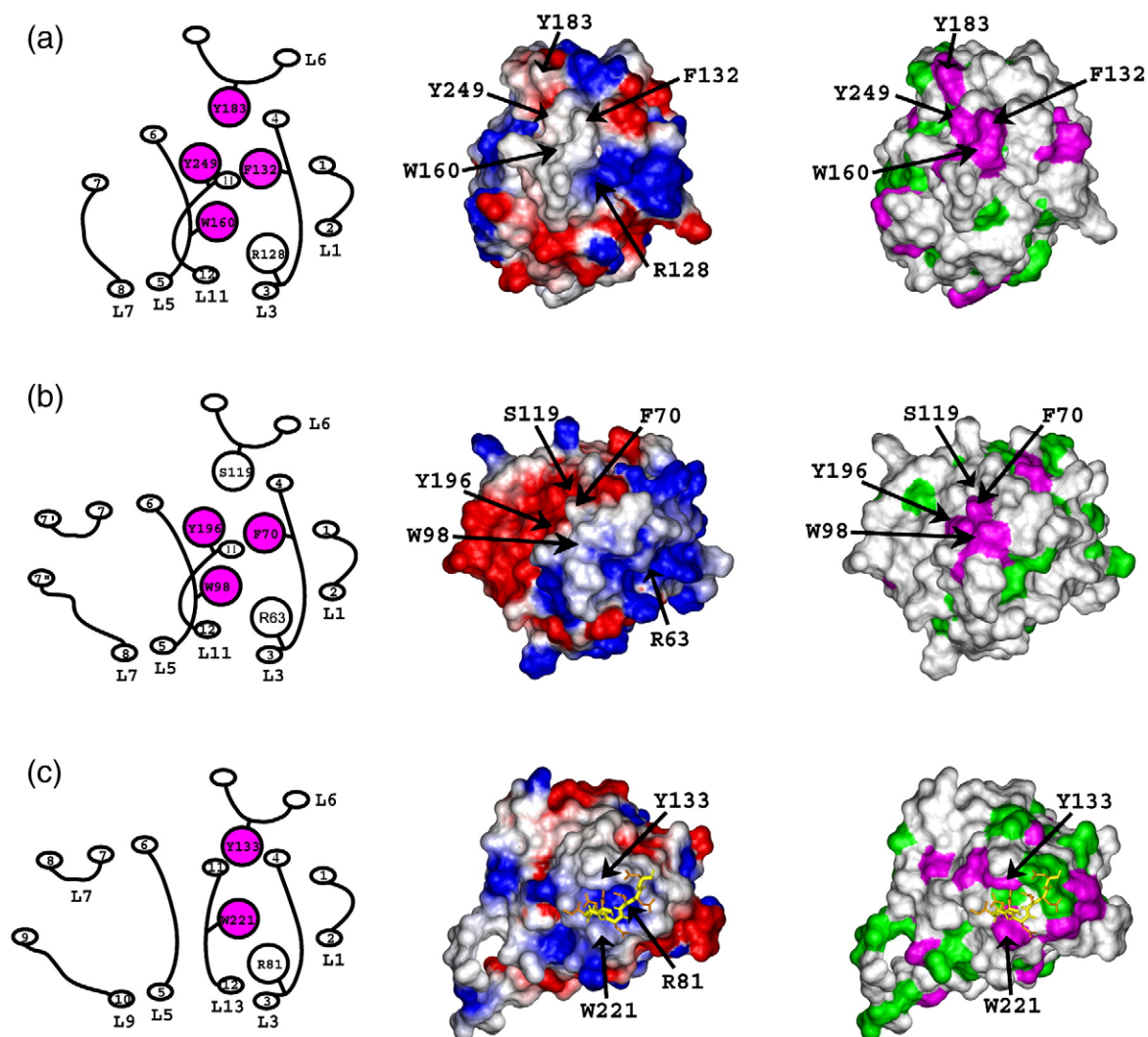


Fig. 9. Representations of the binding interfaces of the NHR1 domains of Neur and KIAA1787, and the B30.2/SPRY domain. (a) Left: a cartoon representation of the loops with crucial residues (R128, F132, W160, Y183, and Y249) at the bottom area of the β -sandwich fold of the Neur NHR1 domain. Electrostatic (middle) and hydrophobic (right) surfaces of the Neur NHR1 domain are shown. (b) Left: a cartoon representation of the loops with crucial residues (R63, F70, W98, Y196, and S119) at the bottom area of the β -sandwich fold of the KIAA1787 NHR1 domain. Electrostatic (middle) and hydrophobic (right) surfaces of the KIAA1787 NHR1 domain are shown. (c) Left: a cartoon representation of the loops with crucial residues (R81, Y133, and W221) at the bottom area of the β -sandwich fold of the B30.2/SPRY domain of GUSTAVUS. Electrostatic (middle) and hydrophobic (right) surfaces of the B30.2/SPRY domain of GUSTAVUS complexed with a VASA peptide²² are shown. The orientations of the molecules represent a -90° rotation on the y -axis from the left diagram in Fig. 5b. On all of the hydrophobic surfaces, the aromatic and aliphatic residues are shown in magenta and green, respectively.

site for the target peptide (Fig. 9c). In this B30.2/SPRY domain, the segment corresponding to the long L6 loop in the Neur NHR1 domain forms the β -strand that associates with the β 4-strand and is involved in the formation of the upper concave β -sheet. Thus, the Tyr133 residue on the L6 loop is proximal to the β 13 strand and can form the proper binding pocket with Trp221 on the L13 loop (Fig. 9c). In the case of the Neur NHR1 domain (Fig. 9a), Tyr133 and Trp221 in the B30.2/SPRY domain are not conserved. Instead, the Trp160 residue on the L5 loop in the Neur NHR1 domain is located between the L3 and L11 loops, where it occupies the space

corresponding to Trp221 in the B30.2/SPRY domain. Furthermore, in the Neur NHR1 domain, the Tyr249 residue in the β 11 strand occupies the space corresponding to Tyr133 on the L6 loop in the B30.2/SPRY domain. The Neur NHR1 domain also has a Tyr183 residue residing at the tip of the L6 loop, as in the B30.2/SPRY domain. However, it is located above the five-stranded concave β -sheet. Another characteristic point of the Neur NHR1 domain, as compared to the B30.2/SPRY domain, is the presence of the Phe132 residue on the L3 loop, which narrows the space formed between Trp160 and Tyr183 (Fig. 9).

The present NMR study has indicated that the NHR domains and the B30.2/SPRY domains belong to related protein families, and the target binding sites of the Neur NHR1 domain and the B30.2/SPRY domains are situated in comparable regions on the surfaces of the similar tertiary structures. However, the characteristic surface structures, composed of the L3, L5, and L11 (L13) loops, as well as the tip of the L6 loop, provide the individual target specificity for each member of these domain families.

Conclusion

The solution structures of the two NHR domains of Neur and KIAA1787 were determined by NMR spectroscopy in this study. The interactions between the Neur NHR1 domain and a Tom peptide were confirmed by NMR titration and ITC experiments, and the binding site was mapped on the solution structure. The Neur NHR1 domain shares a similar 3D structure and binding interface location with the B30.2/SPRY domains. Nevertheless, these domains show high specificity for their respective targets in protein–protein interactions. The Tom peptide inhibits the binding between Neur and the Notch ligand, Delta. However, the determination of whether the Neur NHR1 domain uses the same binding site for both Delta and Tom will await future experiments to elucidate the control mechanism of the Notch signaling system.

Materials and Methods

Screening of folded protein

Firstly, we evaluated the protein expression for different Neur constructs with around 60, 120, and 160 amino acid residues, using GFP as a C-terminal fusion,^{40,41} in a batch mode with our cell-free protein synthesis system.^{42,43} As for the core constructs with 60, 120, and 160 amino acids, the regions spanning residues 106–166, 106–226, and 106–266 were defined, respectively. On the basis of these core regions, the constructs with 10 additional or fewer amino acid residues at the N- and/or C-termini were also designed for screening (Fig. S1 shows the example for the constructs with 160 amino acids). When the translated products of these constructs were properly folded, it is highly possible that the C-terminally fused GFP was also properly folded, and thus the GFP-related fluorescence was measured in the reaction mixtures.

Along with the above-mentioned GFP screening, we identified the domain boundaries by checking the solubility of the translated products for the targeted constructs. Namely, the selected constructs with different N-terminal His-tags (NHis-tag or N11-tag) were tested. The total and soluble fractions were subjected to SDS-PAGE, and the solubility of the proteins was confirmed. Finally, uniformly ¹⁵N-labeled protein samples with a His-tag were synthesized by the middle-scale dialysis mode of the cell-free reaction. The proteins were partially purified by chromatography on nickel–Sepharose resin (GE Healthcare). The folding of the proteins was examined by measuring their 2D ¹H–¹⁵N HSQC spectra.

Preparation of protein samples

The ¹⁵N/¹³C-labeled NHR1 domain samples of Neur and KIAA1787 were synthesized using an *Escherichia coli* cell-free protein synthesis system^{42,43} and were treated and purified as described previously.⁵⁹ The engineered NHR1 domains of Neur and the human KIAA1787 protein comprised 161 amino acid residues, Pro106–Gln266, and 163 amino acid residues, Glu43–Leu205, respectively, including seven N-terminal, nonnative residues (GSSGSSG). For the structure determination, uniformly ¹⁵N/¹³C-labeled samples were concentrated to 1.05 mM for Neur NHR1 and 1.10 mM for KIAA1787 NHR1, in 20 mM Tris–HCl buffer (pH 7.0), containing 100 mM NaCl, 1 mM dithiothreitol, and 0.02% NaN₃ with the addition of ²H₂O to 10% (v/v).

NMR spectroscopy

All NMR data were acquired at 25 °C on Bruker AVANCE 600 and AVANCE 800-MHz spectrometers equipped with pulsed field gradient triple-resonance probes. The raw NMR data were processed using the NMRPipe software package.⁶⁰ Linear prediction was used in the ¹⁵N and ¹³C dimensions to improve the digital resolution. Backbone and side-chain ¹H, ¹⁵N, and ¹³C resonances of the NHR domains were assigned by standard double- and triple-resonance NMR experiments.⁶¹ Sequence-specific backbone assignments were achieved with 2D ¹H–¹⁵N HSQC and 3D HNCO, HN(CA)CO, HNCA, HN(CO)CA, CBCA(CO)NH, and HNCACB spectra. Assignments of side-chain resonances were obtained from 2D ¹H–¹³C HSQC and 3D HBHA(CO)NH, HC(CCO)NH, C(CCO)NH, H(C)CH-COSY (correlated spectroscopy), H(C)CH-TOCSY (total COSY), and (H)CCH-TOCSY. The chemical shifts were confirmed by 3D ¹⁵N- and ¹³C-edited NOESY–HSQC spectra with a mixing time of 80 ms. The NMR spectra were analyzed using the programs NMRView⁶² and Kujira.⁶³

Structure calculation

The 3D structures of the NHR1 domains of Neur and KIAA1787 were determined with the program CYANA, which implements automated NOE assignments and structure calculations with torsion angle dynamics.^{46,64} NOE peaks from ¹⁵N- and ¹³C-edited 3D NOESY spectra with an 80-ms mixing time were converted to distance restraints for the structure calculations. Restraints for the backbone torsion angles ϕ and φ were determined by a chemical shift database analysis with the program TALOS.⁴⁸ A total of 2984 and 4011 NOE-derived distance restraints, as well as 146 and 158 dihedral angle restraints, were used for the structure calculations of the Neur NHR1 domain and the KIAA1787 NHR1 domain, respectively. Restraints for backbone–backbone hydrogen bonds in secondary structures were introduced in the final stage of refinement. Furthermore, stereospecific assignments for the isopropyl methyl and methylene groups were determined with CYANA.^{46,47} Starting from 100 extended conformers, final ensembles of 20 conformers were selected on the basis of the lowest final CYANA target function values. The 20 structures from the CYANA calculation were further refined by minimization with AMBER9ll, using the generalized Born mode to obtain the final structures. During the AMBER calculations, the distances and the dihedral angles were subjected to force constants of 32 kcal mol⁻¹ Å⁻¹ and 60 kcal mol⁻¹ rad⁻²,

respectively. The quality of the structures was analyzed using the programs CYANA, PROCHECK-NMR,⁴⁹ and MOLMOL,⁶⁵ and the latter program was also used to prepare drawings of the structures.

NMR titration of the NHR1 domains with a 20-residue Tom peptide and an 8-residue VASA peptide

For the titration experiments, we selected the 20-residue peptide (AASCDNMANEELQRLYTDL) from motif 2 of the Tom protein (residues 72–91) and the eight-residue peptide (DDINNNNN) derived from the VASA protein (residues 183–190). NMR titration experiments were performed by adding the unlabeled peptide solutions to the uniformly ¹⁵N/¹³C-labeled NHR1 domains. The molar protein–peptide ratios were 1:0.1, 0.2, 0.5, 0.7, 1.0, 1.2, 1.5, and 2.0. The 2D ¹H–¹⁵N HSQC and ¹H–¹³C HSQC spectra were measured at each titration step, and the chemical shift changes of the signals were monitored. These 2D spectra were processed with the NMRPipe software⁶⁰ and were analyzed with the program Sparky (T. D. Goddard and D. G. Kneller, SPARKY 3, University of California, San Francisco). The weighted change of the backbone amide proton (HN) and nitrogen (N) chemical shifts was calculated according to the equation: $\Delta\delta = [(\Delta\text{HN})^2 + (\Delta\text{N}/6.5)^2]^{1/2}$.⁵⁸

ITC Measurements

ITC measurements were performed with a MicroCal VP-ITC isothermal titration calorimeter (Micro-Cal, Inc.). The same buffer as for the NMR samples, but without DTT, was used for the ITC measurements. Since the reducing agent (DTT) generated an erratic baseline during the ITC measurements and the duration of the ITC measurements was relatively short, as compared to that of the NMR measurements, DTT was not used in the ITC experiments. The concentrations of the Neur NHR1 domain and the 20-residue Tom peptide were 0.0346 and 0.624 mM, respectively, as determined by UV spectroscopy at 280 nm. A degassed sample of NHR1 was maintained at 25 °C and stirred at 307 rpm in a 1.4-ml reaction cell. For each titration, 5- μ l aliquots of the Tom peptide were added to the NHR1 solution at 240-s intervals to allow complete equilibration. Heat transfer was measured as a function of elapsed time. The heat of dilution, obtained by titrating the identical peptide solution into the reaction cell containing only the buffer, was subtracted prior to analysis. The corrected titration curve was fitted with a one-site model, and the thermodynamic parameters were calculated using the Origin software (version 7.0) provided by MicroCal. The samples of the mutant Neur NHR1 domain (Y183S) and the 20-residue Tom peptide were prepared in the same manner, and the concentrations of the two samples were 0.0377 and 0.667 mM, respectively. The ITC experiment for the mutant was performed in the same manner as that for the wild-type Neur NHR1 domain.

Phylogenetic analysis

The amino acid sequences of the NHR domains were defined on the basis of the domain boundaries from the present structural analysis. We then selected the amino acid sequences of typical NHR-containing proteins in the Pfam database and aligned them using the Clustal X program⁶⁶ (Fig. S2). The phylogenetic tree was con-

structed by the neighbor-joining method, using the Phylodendron program[†].

PDB accession codes

The atomic coordinates for the ensembles of 20 NMR conformers that represent the solution structures of the NHR1 domains of Neur and KIAA1878 have been deposited in the PDB with the accession codes 2YUE and 2E63, respectively.

Acknowledgements

We are grateful to Takayoshi Matsuda, Yasuko Tomo, Masaaki Aoki, Eiko Seki, Kazuharu Hanada, Masaomi Ikari, Yukiko Fujikura, and Takeshi Nagira for preparing the samples and to Dr. Takuma Kasai for his assistance with the ITC experiments. This work was supported by the RIKEN Structural Genomics/Proteomics Initiative, the National Project on Protein Structural and Functional Analyses of the Ministry of Education, Culture, Sports, Science and Technology of Japan. P.G. was supported by a Grant-in-Aid for Scientific Research of the Japan Society for the Promotion of Science and by the Volkswagen Foundation.

Supplementary Data

Supplementary data associated with this article can be found, in the online version, at [doi:10.1016/j.jmb.2009.08.020](https://doi.org/10.1016/j.jmb.2009.08.020)

References

1. Bray, S. J. (2006). Notch signalling: a simple pathway becomes complex. *Nat. Rev. Mol. Cell Biol.* **7**, 678–689.
2. Fiuza, U. M. & Arias, A. M. (2007). Cell and molecular biology of Notch. *J. Endocrinol.* **194**, 459–474.
3. Lai, E. C. (2004). Notch signaling: control of cell communication and cell fate. *Development*, **131**, 965–973.
4. Sanchez-Irizarry, C., Carpenter, A. C., Weng, A. P., Pear, W. S., Aster, J. C. & Blacklow, S. C. (2004). Notch subunit heterodimerization and prevention of ligand-independent proteolytic activation depend, respectively, on a novel domain and the LNR repeats. *Mol. Cell. Biol.* **24**, 9265–9273.
5. Boulianne, G. L., de la Concha, A., Campos-Ortega, J. A., Jan, L. Y. & Jan, Y. N. (1993). The *Drosophila* neurogenic gene neuralized encodes a novel protein and is expressed in precursors of larval and adult neurons. *EMBO J.* **12**, 2586.
6. Yeh, E., Dermer, M., Commisso, C., Zhou, L., McGlade, C. J. & Boulianne, G. L. (2001). Neuralized functions as an E3 ubiquitin ligase during *Drosophila* development. *Curr. Biol.* **11**, 1675–1679.

[†]<http://iubio.bio.indiana.edu/soft/>

7. Itoh, M., Kim, C. H., Palardy, G., Oda, T., Jiang, Y. J., Maust, D. *et al.* (2003). Mind bomb is a ubiquitin ligase that is essential for efficient activation of Notch signaling by Delta. *Dev. Cell*, **4**, 67–82.
8. Deblandre, G. A., Lai, E. C. & Kintner, C. (2001). *Xenopus* neuralized is a ubiquitin ligase that interacts with XDelta1 and regulates Notch signaling. *Dev. Cell*, **1**, 795–806.
9. Pavlopoulos, E., Pitsouli, C., Klueg, K. M., Muskavitch, M. A., Moschonas, N. K. & Delidakis, C. (2001). Neuralized encodes a peripheral membrane protein involved in delta signaling and endocytosis. *Dev. Cell*, **1**, 807–816.
10. Lai, E. C., Deblandre, G. A., Kintner, C. & Rubin, G. M. (2001). *Drosophila* neuralized is a ubiquitin ligase that promotes the internalization and degradation of delta. *Dev. Cell*, **1**, 783–794.
11. Wang, W. & Struhl, G. (2005). Distinct roles for Mind bomb, Neuralized and Epsin in mediating DSL endocytosis and signaling in *Drosophila*. *Development*, **132**, 2883–2894.
12. Le Borgne, R. & Schweisguth, F. (2003). Notch signaling: endocytosis makes delta signal better. *Curr. Biol.* **13**, R273–R275.
13. Le Borgne, R. & Schweisguth, F. (2003). Unequal segregation of Neuralized biases Notch activation during asymmetric cell division. *Dev. Cell*, **5**, 139–148.
14. Bingham, S., Chaudhari, S., Vanderlaan, G., Itoh, M., Chitnis, A. & Chandrasekhar, A. (2003). Neurogenic phenotype of mind bomb mutants leads to severe patterning defects in the zebrafish hindbrain. *Dev. Dyn.* **228**, 451–463.
15. Pitsouli, C. & Delidakis, C. (2005). The interplay between DSL proteins and ubiquitin ligases in Notch signaling. *Development*, **132**, 4041–4050.
16. Le Borgne, R., Remaud, S., Hamel, S. & Schweisguth, F. (2005). Two distinct E3 ubiquitin ligases have complementary functions in the regulation of delta and serrate signaling in *Drosophila*. *PLoS Biol.* **3**, e96.
17. Lai, E. C. (2002). Protein degradation: four E3s for the notch pathway. *Curr. Biol.* **12**, R74–R78.
18. Artavanis-Tsakonas, S., Rand, M. D. & Lake, R. J. (1999). Notch signaling: cell fate control and signal integration in development. *Science*, **284**, 770–776.
19. Le Borgne, R. (2006). Regulation of Notch signalling by endocytosis and endosomal sorting. *Curr. Opin. Cell Biol.* **18**, 213–222.
20. Chitnis, A. (2006). Why is delta endocytosis required for effective activation of notch? *Dev. Dyn.* **235**, 886–894.
21. Le Borgne, R., Bardin, A. & Schweisguth, F. (2005). The roles of receptor and ligand endocytosis in regulating Notch signaling. *Development*, **132**, 1751–1762.
22. Woo, J. S., Suh, H. Y., Park, S. Y. & Oh, B. H. (2006). Structural basis for protein recognition by B30.2/SPRY domains. *Mol. Cell*, **24**, 967–976.
23. Gouet, P., Courcelle, E., Stuart, D. I. & Metz, F. (1999). ESPript: analysis of multiple sequence alignments in PostScript. *Bioinformatics*, **15**, 305–308.
24. Price, B. D., Chang, Z., Smith, R., Bockheim, S. & Laughon, A. (1993). The *Drosophila* neuralized gene encodes a C3HC4 zinc finger. *EMBO J.* **12**, 2411–2418.
25. Boulianne, G. L., de la Concha, A., Campos-Ortega, J. A., Jan, L. Y. & Jan, Y. N. (1991). The *Drosophila* neurogenic gene neuralized encodes a novel protein and is expressed in precursors of larval and adult neurons. *EMBO J.* **10**, 2975–2983.
26. Commisso, C. & Boulianne, G. L. (2007). The NHR1 domain of Neuralized binds Delta and mediates Delta trafficking and Notch signaling. *Mol. Biol. Cell*, **18**, 1–13.
27. Lai, E. C. & Rubin, G. M. (2001). Neuralized is essential for a subset of Notch pathway-dependent cell fate decisions during *Drosophila* eye development. *Proc. Natl Acad. Sci. USA*, **98**, 5637–5642.
28. Yeh, E., Zhou, L., Rudzik, N. & Boulianne, G. L. (2000). Neuralized functions cell autonomously to regulate *Drosophila* sense organ development. *EMBO J.* **19**, 4827–4837.
29. Lehmann, R., Jiménez, F., Dietrich, U. & Campos-Ortega, J. A. (1983). On the phenotype and development of mutants of early neurogenesis in *Drosophila melanogaster*. *Dev. Genes Evol.* **192**, 62–74.
30. De Renzis, S., Yu, J., Zinzen, R. & Wieschaus, E. (2006). Dorsal-ventral pattern of Delta trafficking is established by a Snail-Tom-Neuralized pathway. *Dev. Cell*, **10**, 257–264.
31. Bardin, A. J. & Schweisguth, F. (2006). Bearded family members inhibit Neuralized-mediated endocytosis and signaling activity of Delta in *Drosophila*. *Dev. Cell*, **10**, 245–255.
32. Lai, E. C., Bodner, R. & Posakony, J. W. (2000). The enhancer of split complex of *Drosophila* includes four Notch-regulated members of the bearded gene family. *Development*, **127**, 3441–3455.
33. Lai, E. C., Bodner, R., Kavalier, J., Freschi, G. & Posakony, J. W. (2000). Antagonism of notch signaling activity by members of a novel protein family encoded by the bearded and enhancer of split gene complexes. *Development*, **127**, 291–306.
34. Larsen, L. & Ropke, C. (2002). Suppressors of cytokine signalling: SOCS. *Acta Pathol., Microbiol. Immunol. Scand.* **110**, 833–844.
35. Hu, Y., Nguyen, T. T., Bui, K. C., Demello, D. E. & Smith, J. B. (2005). A novel inflammation-induced ubiquitin E3 ligase in alveolar type II cells. *Biochem. Biophys. Res. Commun.* **333**, 253–263.
36. Lai, E. C. & Rubin, G. M. (2001). Neuralized functions cell-autonomously to regulate a subset of notch-dependent processes during adult *Drosophila* development. *Dev. Biol.* **231**, 217–233.
37. Wu, G., Liu, C. & He, X. (2004). Ozz; a new name on the long list of beta-catenin's nemeses. *Mol. Cell*, **13**, 451–453.
38. Nastasi, T., Bongiovanni, A., Campos, Y., Mann, L., Toy, J. N., Bostrom, J. *et al.* (2004). Ozz-E3, a muscle-specific ubiquitin ligase, regulates beta-catenin degradation during myogenesis. *Dev. Cell*, **6**, 269–282.
39. Kile, B. T., Schulman, B. A., Alexander, W. S., Nicola, N. A., Martin, H. M. & Hilton, D. J. (2002). The SOCS box: a tale of destruction and degradation. *Trends Biochem. Sci.* **27**, 235–241.
40. Kigawa, T., Inoue, M., Aoki, M., Matsuda, T., Yabuki, T., Seki, E. *et al.* (2007). The use of the *Escherichia coli* cell-free protein synthesis for structural biology and structural proteomics. In *Cell-Free Protein Synthesis: Methods and Protocols* (Spirin, A. S. & Swartz, J. R., eds), Wiley-VCH, Weinheim, Germany.
41. Kukimoto-Niino, M., Takagi, T., Akasaka, R., Murayama, K., Uchikubo-Kamo, T., Terada, T. *et al.* (2006). Crystal structure of the RUN domain of the RAP2-interacting protein x. *J. Biol. Chem.* **281**, 31843–31853.
42. Kigawa, T., Yabuki, T., Matsuda, N., Matsuda, T., Nakajima, R., Tanaka, A. & Yokoyama, S. (2004). Preparation of *Escherichia coli* cell extract for highly productive cell-free protein expression. *J. Struct. Funct. Genomics*, **5**, 63–68.

43. Matsuda, T., Koshiba, S., Tochio, N., Seki, E., Iwasaki, N., Yabuki, T. *et al.* (2007). Improving cell-free protein synthesis for stable-isotope labeling. *J. Biomol. NMR*, **37**, 225–229.
44. Wüthrich, K. (1986). *NMR of Proteins and Nucleic Acids*. Wiley, New York.
45. Schubert, M., Labudde, D., Oschkinat, H. & Schmieder, P. (2002). A software tool for the prediction of Xaa-Pro peptide bond conformations in proteins based on ¹³C chemical shift statistics. *J. Biomol. NMR*, **24**, 149–154.
46. Güntert, P., Mumenthaler, C. & Wüthrich, K. (1997). Torsion angle dynamics for NMR structure calculation with the new program DYANA. *J. Mol. Biol.* **273**, 283–298.
47. Güntert, P. (2004). Automated NMR structure calculation with CYANA. *Methods Mol. Biol.* **278**, 353–378.
48. Cornilescu, G., Delaglio, F. & Bax, A. (1999). Protein backbone angle restraints from searching a database for chemical shift and sequence homology. *J. Biomol. NMR*, **13**, 289–302.
49. Laskowski, R. A., Rullmann, J. A., MacArthur, M. W., Kaptein, R. & Thornton, J. M. (1996). AQUA and PROCHECK-NMR: programs for checking the quality of protein structures solved by NMR. *J. Biomol. NMR*, **8**, 477–486.
50. Holm, L., Kaariainen, S., Rosenstrom, P. & Schenkel, A. (2008). Searching protein structure databases with DaliLite v.3. *Bioinformatics*, **24**, 2780–2781.
51. Woo, J. S., Imm, J. H., Min, C. K., Kim, K. J., Cha, S. S. & Oh, B. H. (2006). Structural and functional insights into the B30.2/SPRY domain. *EMBO J.* **25**, 1353–1363.
52. Babon, J. J., Sabo, J. K., Zhang, J. G., Nicola, N. A. & Norton, R. S. (2009). The SOCS box encodes a hierarchy of affinities for Cullin5: implications for ubiquitin ligase formation and cytokine signalling suppression. *J. Mol. Biol.* **387**, 162–174.
53. Grütter, C., Briand, C., Capitani, G., Mittl, P. R., Papin, S., Tschopp, J. & Grütter, M. G. (2006). Structure of the PRYSPRY-domain: implications for autoinflammatory diseases. *FEBS Lett.* **580**, 99–106.
54. Keeble, A. H., Khan, Z., Forster, A. & James, L. C. (2008). TRIM21 is an IgG receptor that is structurally, thermodynamically, and kinetically conserved. *Proc. Natl Acad. Sci. USA*, **105**, 6045–6050.
55. Nicholson, S. E. & Hilton, D. J. (1998). The SOCS proteins: a new family of negative regulators of signal transduction. *J. Leukoc. Biol.* **63**, 665–668.
56. Wang, D., Li, Z., Schoen, S. R., Messing, E. M. & Wu, G. (2004). A novel MET-interacting protein shares high sequence similarity with RanBPM, but fails to stimulate MET-induced Ras/Erk signaling. *Biochem. Biophys. Res. Commun.* **313**, 320–326.
57. Wang, D., Li, Z., Messing, E. M. & Wu, G. (2005). The SPRY domain-containing SOCS box protein 1 (SSB-1) interacts with MET and enhances the hepatocyte growth factor-induced Erk-Elk-1-serum response element pathway. *J. Biol. Chem.* **280**, 16393–16401.
58. Mulder, F. A., Schipper, D., Bott, R. & Boelens, R. (1999). Altered flexibility in the substrate-binding site of related native and engineered high-alkaline *Bacillus subtilis*ins. *J. Mol. Biol.* **292**, 111–123.
59. Li, H., Koshiba, S., Hayashi, F., Tochio, N., Tomizawa, T., Kasai, T. *et al.* (2008). Structure of the C-terminal phosphotyrosine interaction domain of Fe65L1 complexed with the cytoplasmic tail of amyloid precursor protein reveals a novel peptide binding mode. *J. Biol. Chem.* **283**, 27165–27178.
60. Delaglio, F., Grzesiek, S., Vuister, G. W., Zhu, G., Pfeifer, J. & Bax, A. (1995). NMRPipe: a multidimensional spectral processing system based on UNIX pipes. *J. Biomol. NMR*, **6**, 277–293.
61. Clore, G. M. & Gronenborn, A. M. (1998). New methods of structure refinement for macromolecular structure determination by NMR. *Proc. Natl Acad. Sci. USA*, **95**, 5891–5898.
62. Johnson, B. A. & Blevins, R. A. (1994). NMR View: a computer program for the visualization and analysis of NMR data. *J. Biomol. NMR*, **4**, 603–614.
63. Kobayashi, N., Iwahara, J., Koshiba, S., Tomizawa, T., Tochio, N., Güntert, P. *et al.* (2007). KUJIRA, a package of integrated modules for systematic and interactive analysis of NMR data directed to high-throughput NMR structure studies. *J. Biomol. NMR*, **39**, 31–52.
64. Herrmann, T., Güntert, P. & Wüthrich, K. (2002). Protein NMR structure determination with automated NOE assignment using the new software CANDID and the torsion angle dynamics algorithm DYANA. *J. Mol. Biol.* **319**, 209–227.
65. Koradi, R., Billeter, M. & Wüthrich, K. (1996). OLMOL: a program for display and analysis of macromolecular structures. *J. Mol. Graphics*, **14**, 51–55.
66. Thompson, J. D., Gibson, T. J., Plewniak, F., Jeanmougin, F. & Higgins, D. G. (1997). The CLUSTAL_X windows interface: flexible strategies for multiple sequence alignment aided by quality analysis tools. *Nucleic Acids Res.* **25**, 4876–4882.